To seal a wound, caterpillars transform blood from a viscous to a viscoelastic fluid in a few seconds

Pavel Aprelev[1#], Artis Brasovs[1#], Terri F. Bruce[2], Charles E. Beard[3], Peter H. Adler[3], and Konstantin G. Kornev*[1]

[1]Department of Materials Science and Engineering, Clemson University, Clemson, South Carolina, USA, 29634. E-mail: kkornev@clemson.edu

[2]Light Imaging Facility, Clemson University, Clemson, South Carolina, USA, 29634

[3]Department of Plant and Environmental Sciences, Clemson University, Clemson, South Carolina USA, 29634

[#] Equal contribution to the work

Keywords: cell aggregation, hemolymph, hemocytes, clotting kinetics, Lepidoptera, rheology, viscosity, surface tension, adhesion

Abstract

In insects vulnerable to dehydration, the mechanistic reaction of blood after wounding is rapid. It allows insects to minimize blood loss by sealing the wound and forming primary clots that provide scaffolding for the formation of new tissue. Using nano-rheological magnetic rotational spectroscopy with nickel nanorods and extensional rheology, we studied the properties of blood dripping from the wound of caterpillars of the Carolina sphinx moth (*Manduca sexta*) with a high concentration of blood cells. We discovered that wound sealing followed a two-step scenario. First, in a few seconds, Newtonian low-viscosity blood turns into a non-Newtonian viscoelastic fluid that minimizes blood loss by retracting dripping blood back to the wound. Next, blood cells aggregate, starting from the interfaces and propagating inwardly. We studied these processes using optical phase-contrast and polarized microscopy, X-ray imaging, and modeling. Comparative analyses of the cell-rich and cell-poor blood of different insects revealed common features of blood behavior. These discoveries can help design fast-working thickeners for vertebrate blood, including human blood.

1. INTRODUCTION

Insects developed special strategies to deal with wounding and potential infection[1-9]. Wounding triggers humoral and cellular reactions associated with insect blood (hemolymph) [1-11]. These reactions span spatial scales from nanometer to microscopic and time scales from microseconds to hours. At the wound site, a primary clot nucleates within minutes after wounding[1, 2], while formation of a scab and new epidermal tissue happen on a time scale more than two orders of magnitude greater [1, 2, 12]. The physical features of primary clot formation in the first minutes of hemolymph leakage from the wound are not sufficiently detailed, and only recently was a quantitative analysis of the kinetics of clot nucleation in cell-rich hemolymph reported [13].

The concentration of cells (hemocytes) in the blood of different insect species varies significantly; hence, insects developed various strategies for wound sealing. In the hemocyte-poor hemolymph, as in butterflies and moths, the humoral reactions in plasma cause self-assembly of lipoproteins[11, 14-16]. Lipoproteins, with their surfactant-like action, recognize the foreign interface and immediately engage hemocytes or other large proteins such as hemocytin (molecular weights of hemocytin in the moth *Bombyx mori* and fly *Drosophila melanogaster* are ~260 and~300 KDa, respectively)[17] to aggregate into filamentary threads consisting of more complex biopolymer subunits [20] and then into gel-like wound covers [10, 11]. The gel's tightening of the hemocytes at the wound surface renders the complex mesh impermeable to microorganisms and hinders water evaporation.

Lipoproteins are also found in the primary clots of hemocyte-rich hemolymph [6, 7, 18-23], such as exchangeable Apolipophorin-III in the cockroach *Periplaneta americana*[6, 24]. In contrast to the hemocyte-poor blood of butterflies and moths (Lepidoptera), the hemolymph of their larvae (i.e., caterpillars) is hemocyte-rich. The comparative biomolecular studies of clotting in lepidopteran larvae and adults and in other insects suggests that the hemocytin and lipoproteins common for adults and larvae could be among the first to respond and trigger complex immune reactions resulting in the formation of filamentary structures and primary clots [7, 16, 17, 20-23, 25, 26].

The limiting step for primary clot formation in larvae of the Carolina sphinx moth (*Manduca sexta*) is aggregation of hemolymph cells (hemocytes), assisted by pseudopodia, the thread-like extensions of the hemocytes[27]. In larvae of *Manduca sexta*, the cells aggregate in about 3–5 minutes. Within a few minutes later, the cells consolidate and the aggregate stiffens, as manifested by a weak elastic reaction[13] about 4–5 minutes from the moment of aggregation. The primary clot remains soft relative to the repaired wound [12], not only in Lepidoptera, such as *M. sexta*, but also in other insects. In *Drosophila*, for example, primary clots are initially soft and can be pulled from the hemolymph with a metal needle [28]. The biomechanics of primary clot nucleation, consolidation, and stiffening remain poorly understood.

In view of these knowledge gaps, we investigated the material properties of clotting hemolymph to reveal the physical determinants that stop the bleeding. The hemocyte-rich blood of fifth-instar (i.e., mature) larvae of *Manduca sexta* was chosen as our model system.

We first studied the time needed for the insect to react to wounding and to stop the loss of hemocyte-rich hemolymph. For the caterpillars of *M. sexta*, the time to change rheological properties of hemolymph is surprisingly short, only a few seconds. This fast reaction and the small volume of available droplets present a challenge to the investigation of the materials properties of hemolymph. Therefore,

we developed new approaches to study the rheological and surface properties of the drop. The comparative analysis of the short-time clotting phenomena associated with the preliminary sealing of the insect wound revealed a general strategy for wound healing: first, the insect turns Newtonian, almost inviscid hemolymph, into a viscoelastic fluid. The acquired elasticity prevents hemolymph from escaping from the wound. The fluid film or a drop covering the wound surface then forms a crust made from a gel-like biopolymer mesh (in hemocyte-poor hemolymph) or a composite hemocyte-polymer mesh (in hemocyte-rich hemolymph).

2. RESULTS.

2.1. The time to stop bleeding from the wound.

To evaluate the relevant timescale of the formation of a primary clot, we used a setup (Figure 1A) in which the wound was oriented downward and the hemolymph dripped on its own. Caterpillars of 9–10 g and 1–2 days before pre-pupation were used. Each caterpillar was constrained in a tube and hemolymph was extracted via a 1–2 mm incision in the 3rd proleg.

Figure 1. (A) Cylindrical plastic sleeve (1) supported by an X-shaped holder (4). The plastic sleeve has a window exposing a portion of the side of the mid-abdomen of a larva of Manduca sexta with a wounded proleg. The dripping hemolymph formed long filaments (2) with droplets. Hemolymph is collected in a Petri dish (3). (B) The sleeve (1) with the caterpillar is flipped upside down, and a metal ball (5) is brought in contact with the wound to form a hemolymph meniscus. The glass rod (6) with the ball (5) is controlled by a manipulator that allows the ball to be lifted to a prescribed height and form a liquid bridge. (C) The hemolymph filament can be obtained from a pool of hemolymph, using either the same ball (5) as in B) or by applying a rod (6).

This setup allowed us to probe the dripping hemolymph several seconds after making the incision. Filming the features of drop and liquid bridge formation had about a 5% success rate because shortly after incision, the caterpillar moved vigorously, causing difficulties for focusing the camera. Nonetheless, our naked-eye observations and filming confirmed that in the first several seconds after incision, the detachment of the falling drop from the wound followed the scenario common for simple fluids such as water[29, 30]: the drop formed a liquid bridge connecting it with the wound (Figure 2A), and then the bridge necked (Figure 2B, C) and broke, producing satellites (Figure 2D, E). This behavior suggested that in the first seconds, mostly water-like, low-viscosity hemolymph dripped from the wound.

During the next 5–10 seconds (i.e., ~ 10–15 seconds after incision), drop detachment showed a different scenario (Figure 3). The necking stage observed in Figure 2B, C proceeded similarly (Figure 3A, B), but after that, instead of breaking up the bridge as in Figure 2D, the hemolymph formed filaments of uniform radius (Figure 3C). Before the breakup, the straight filament formed a bulge in the middle (Figure 3D) and the bulge grew to make a second drop (Figure 3E, F). The droplets moved toward the menisci pulled by the connecting filaments. The filaments that formed 10–15 seconds after incision broke up in ~ 20–40 milliseconds (Figure 3G).

During the next 50–60 seconds (i.e., ~ 75 seconds after incision), drop detachment followed the scenario in Figure 3 (Video S1). However, the lifetime of these late filaments increased significantly, by about 1 order of magnitude, to ~ 240 microseconds.

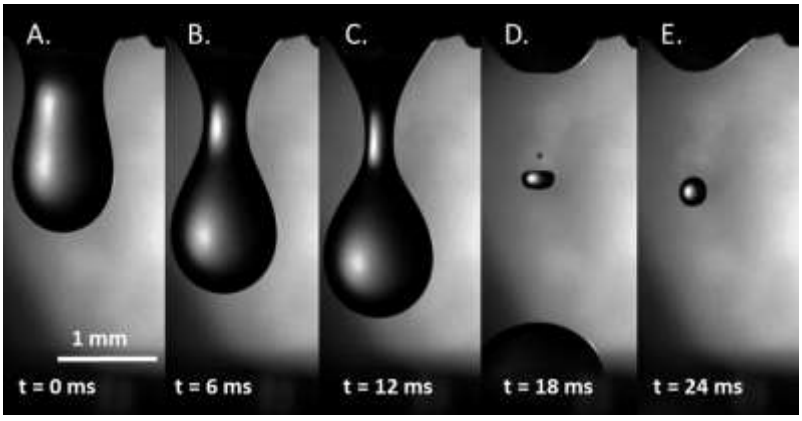

Figure 2. Hemolymph dripping from the wound of a caterpillar several seconds after the wound was made. No filaments were observed, indicating that the hemolymph at this time scale was not highly viscous or elastic.

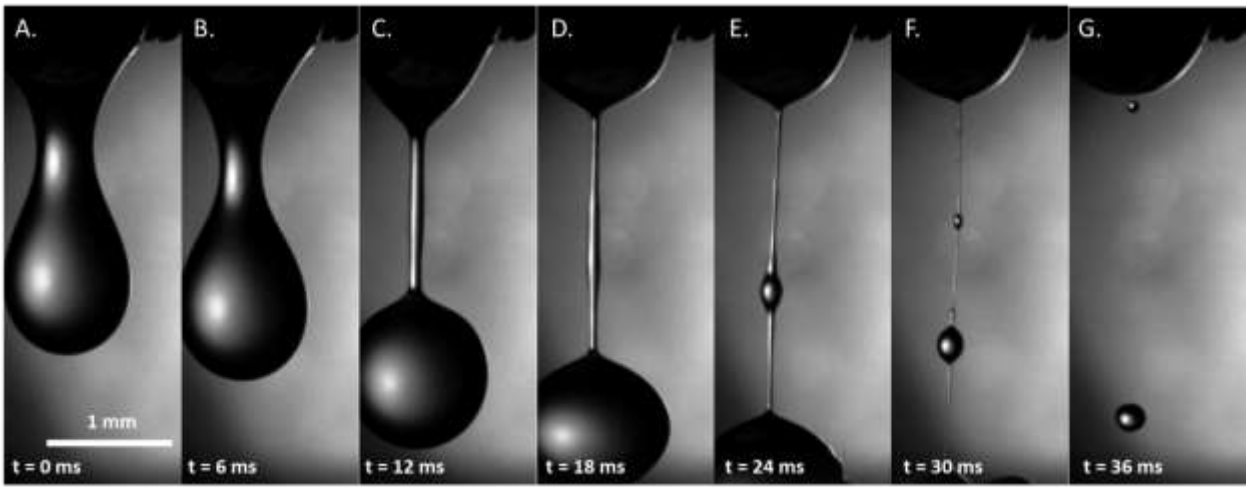

Figure 3. Hemolymph dripping from the wound of a caterpillar within 10-15 seconds after wounding. A straight filament in D) indicates that the hemolymph either increased its viscosity or became viscoelastic.

These results indicate that the properties of hemolymph change quickly: hemolymph starts dripping as an almost inviscid water-like fluid, then quickly changes its rheological properties. Typically, bleeding stopped after 60–90 seconds.

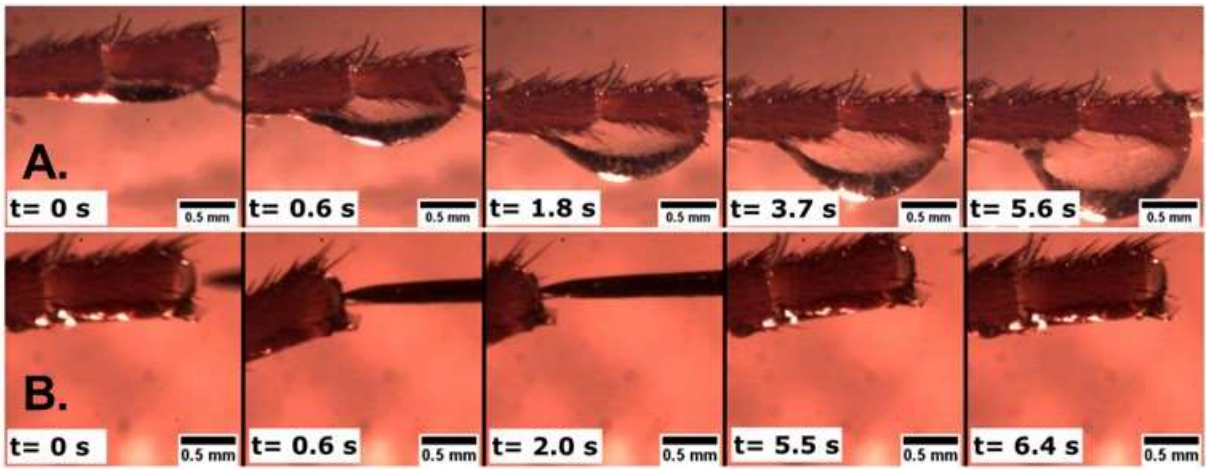

Figure 4. Hemolymph dripping from a severed antenna of the cockroach Periplaneta americana. The head (not pictured) is to the left. (A) After cutting off the end of the antenna, hemolymph continued flowing to this end. Over about 6 seconds, a drop formed. After t=5.6 s, the drop fell, and no other drops appeared. (B) After ~ 10 minutes, the wound was completely sealed by a rigid crust: a tungsten needle was not able to penetrate the crust. When the needle was applied (t=0.6 s) to a cantilevered antenna, the antenna bent, tilting its end as illustrated in the figure. When the needle was removed (t=5.5 s and t=6.4 s), the antenna returned to its original state and the sealed end appeared undeformed.

The scenario of wound sealing in larvae of *M. sexta* was validated with the cockroach *Periplaneta americana* (Figure 4). Although the hemolymph composition of cockroaches could be somewhat different, both insects have hemocyte-rich hemolymph[31] and, as shown below, the plasma viscosity for both species is similar. After detachment of an antennal flagellomere (i.e., an individual unit of the last antennal segment), a drop of hemolymph appeared at the cut end. The drop fell and the remaining hemolymph moved back into the antennal lumen. No other drops appeared and after about 10 minutes, the wound had sealed with a rigid crust.

The almost constant radius of the cylindrical filaments indicated that the hemolymph had either thickened by increasing its shear viscosity or become elastic [30, 32]. In other words, one could think of the filaments as similar to those produced either by thick honey-like fluids or thin dog-saliva-like fluids. To have honey-like filaments, shear viscosity of the hemolymph must increase significantly. We, therefore, measured the shear viscosity by employing Magnetic Rotational Spectroscopy with nickel (Ni) nanorods.

2.2. Characterization of shear viscosity using Magnetic Rotational Spectroscopy with nickel nanorods.

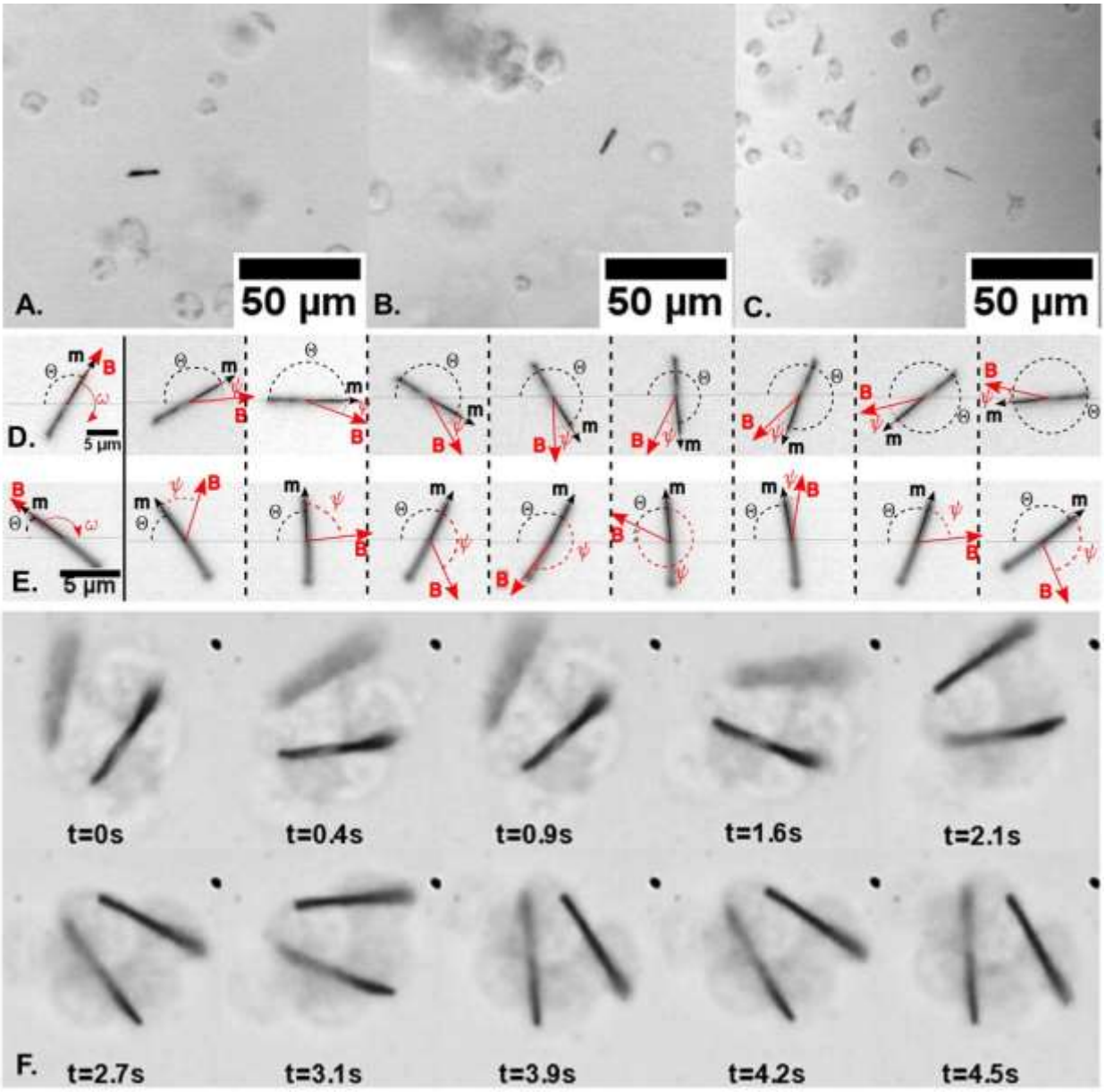

Figure 5. A) Nickel nanorods in a hemolymph drop from larvae of M. sexta. The different nanorods were imaged with a 10x Olympus BX51 objective. The nanorods were observed through the hemolymph-air interface and the images were taken at (A) $t = 5\ minutes$, *(B)* $11\ minutes$, *and (C)* $16\ minutes$ *after drop placement on the glass slide. (D) Synchronous rotation of a nanorod with the applied rotating field. The angle* ψ *that the magnetic moment* $\boldsymbol{m}$ *makes with the field* $\boldsymbol{B}$ *is constant. (E) Asynchronous rotation of a nanorod with the applied rotating field. When the nanorod follows the applied magnetic field, it oscillates so that the angle* ψ *changes with time periodically. (F) Hemocytes attach themselves to the nanorods. Applying a rotating magnetic field, the aggregate can rotate in an asynchronous regime.*

Ferromagnetic nickel nanorods coated with poly(vinylpyrrolidone) were dispersed in a hemolymph drop and forced to continuously rotate by applying a rotating magnetic field and changing the rotating frequency ω_B[13, 33-35]. When an applied rotating magnetic field $\boldsymbol{B}$ acts on a nanorod of magnetization M and volume V, it exerts a torque, $T_B = VMBsin(\omega_B t - \theta)$, forcing the nanorod to turn

in the B-plane. The angle $\psi = \omega_B t - \theta$ specifies the angle that the magnetic moment makes with the magnetic field at time moment t. The magnetic moment is aligned with the nanorod axis, making angle θ with a stationary reference axis (Figure 5).

When a nanorod rotates, it experiences resistance from the surrounding hemolymph. The MRS theory uses the Jeffery[36] model of rotation of an ellipsoid in a Newtonian fluidof viscosity η. Therefore, this technique provides the fluid viscosity at zero shear rate. The torque on the nanorod of length $L_0$and diameter d is written as $T_\eta = \Gamma \eta d\theta/dt$, where $\Gamma = \frac{\pi {L_0}^3}{3\, ln(L_0/d) - 2.4}$ is the nanorod formfactor [37]. For nanorods, the inertial forces at the given frequencies are insignificant; thus, balancing the mechanical and magnetic torques, $T_\eta = T_B$, we model and interpret the observed behavior and rotational dynamics of

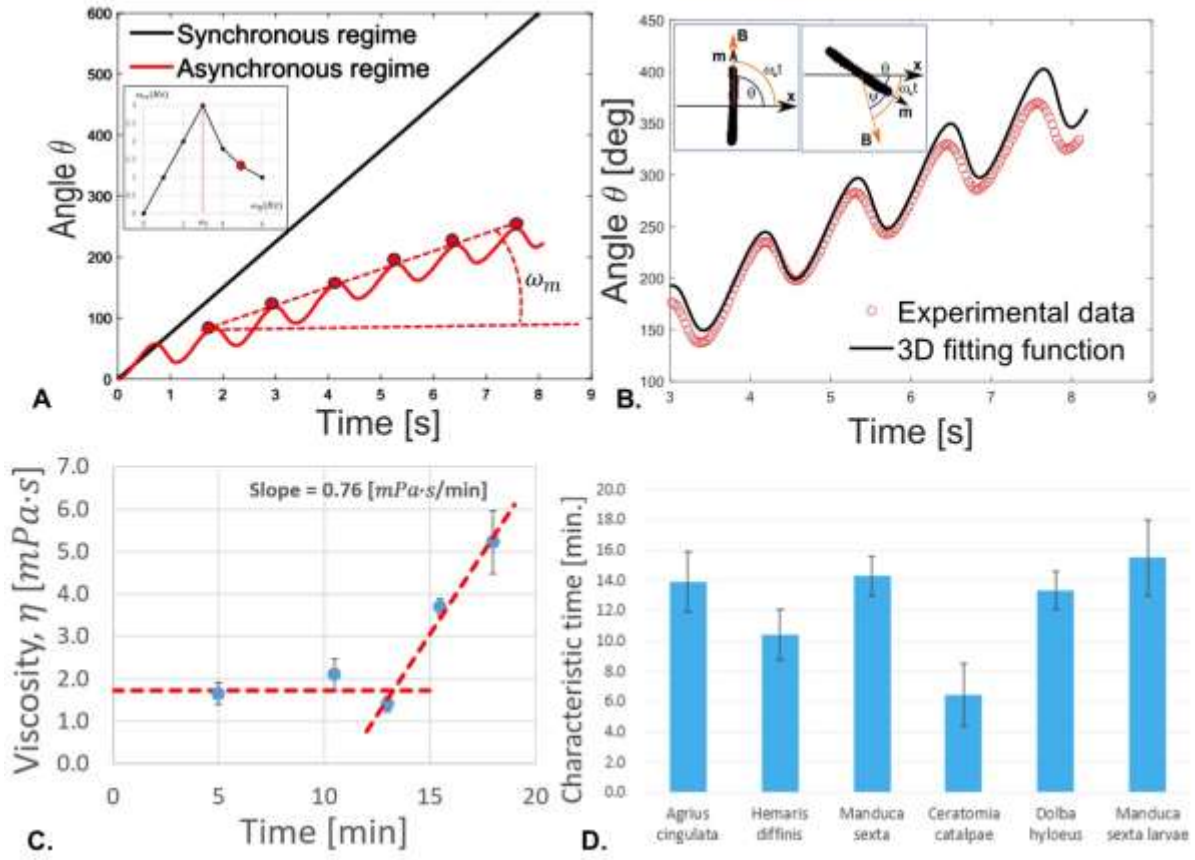

the nanorods in different drops of hemolymph.

*Figure 6. (A) Angular dependence of $\theta(t)$ on time for synchronous (black) and asynchronous (red) rotation of the nanorod. The slope of the dashed line gives an average rate of nanorod revolution ω_m in the asynchronous regime of rotation. The inset illustrates the characteristic master curve used in Magnetic Rotational Spectroscopy. The rate ω_m of rotation of the nanorod is measured as a function of the frequency of rotating field ω_B. When the driving frequency is small, $\omega_B < \omega_c$, the nanorod rotates synchronously with the field, $\omega_m = \omega_B$. When the driving frequency reaches a critical frequency $\omega_B = \omega_c$ and increases further, the nanorod rotation changes to asynchronous mode. The descending curve illustrates the effect of enhanced energy dissipation during asynchronous rotation of the nanorod. The peak value ω_c is easy to detect in experiments. The red dot in the inset corresponds to this slope of the dashed line. (B) In experiments, the magnetic moment **m** of a nanorod is always directed along the nanorod axis. Aligning the moment (and hence the nanorod) parallel to the field **B**, the reference axis x is set perpendicular to the nanorod axis. Then, rotating the field with frequency ω_B, one tracks the angle θ that the nanorod axis makes with the x-axis. During nanorod rotation, the angle ψ that magnetic moment **m** makes with the applied field **B** is not visible. The observed angle θ is then analyzed*

with the model to evaluate the fluid viscosity. In this example, the experimental data on nanorod rotation in hemolymph were satisfactorily explained by modeling hemolymph as a Newtonian fluid with constant viscosity. (C) Viscosity remained constant over minutes. In this example showing the dependence of hemolymph viscosity of M. sexta larvae, viscosity stayed constant for more than 10 minutes and then steeply increased. (D) Measurements of the time when viscosity of different lepidopterans (hawkmoths) increased twice the initial value indicated that the shear viscosity remained constant for at least 5 minutes.

The nanorods were tracked with a camera and the videos were post-processed to fit the nanorod angle versus time, using this model. Two distinguishable scenarios of nanorod rotation are illustrated in Figure 5D, E and Figure 6.

At low driving frequencies, ω_B, the nanorod rotated synchronously, lagging behind the field by a constant angle ψ. When the frequency ω_B increased above a certain critical value $\omega_c = VMB/\Gamma\eta$, the nanorod began to tumble (Figure 6A, B). Measuring ω_c, as explained in Refs.[33, 35, 38, 39], we collected the shear viscosity of hemolymph (Table 1). Hemolymph of all probed species showed Newtonian behavior. The shear viscosity of the probed hemolymph did not change over the first few minutes (Figure 6C, D). When probed by a cone-and-plate viscometer at a greater load, *M. sexta* hemolymph showed Newtonian behavior as well [40]

Table 1. Hemolymph viscosity, body length, body width, and sample size for 19 insect species.

Common names **Lepidoptera species (adults)**	Latin names **Lepidoptera species (adults)**	Hemolymph viscosity, mPa*s	Body length, cm	Body width, cm	Forewing length, cm	Number of individuals	Number of nanorods	Number of measurements
Painted lady butterfly	Vanessa cardui	1.34 ± 0.24	2.11 ± 0.08	0.50 ± 0.10	3.01 ± 0.10	14	43	190
Monarch butterfly	Danaus plexippus	1.44 ± 0.39	3.18 ± 0.13	0.57 ± 0.11	5.16 ± 0.10	9	16	106
Pawpaw sphinx moth	Dolba hyloeus	1.48 ± 0.11	3.40 ± 0.14	0.96 ± 0.08	2.83 ± 0.29	5	15	85
Plebeian sphinx moth	Paratrea plebeja	1.51 ± 0.17	3.43 ± 0.35	0.99 ± 0.10	3.13 ± 0.24	5	11	63
Rustic sphinx moth	Manduca rustica	1.47 ± 0.16	5.47 ± 0.27	1.55 ± 0.15	5.99 ± 0.10	5	16	95
Five-spotted hawkmoth	Manduca quinquemaculata	1.70 ± 0.24	5.31 ± 0.44	1.23 ± 0.13	5.40 ± 0.30	7	26	168
Carolina sphinx moth	Manduca sexta	2.17 ± 0.50	4.55 ± 0.49	1.10 ± 0.06	5.28 ± 0.52	19	49	315
Catalpa sphinx moth	Ceratomia catalpae	2.07 ± 0.33	3.40 ± 0.40	0.91 ± 0.10	4.38 ± 0.48	6	13	72
Pink-spotted hawkmoth	Agrius cingulata	1.85 ± 0.29	5.37 ± 0.50	1.28 ± 0.07	4.80 ± 0.40	5	21	110
Tersa sphinx moth	Xylophanes tersa	1.77 ± 0.29	4.01 ± 0.21	0.85 ± 0.06	3.40 ± 0.20	4	18	99
Pandora sphinx moth	Eumorpha pandorus	1.61 ± 0.14	4.86 ± 0.28	1.10 ± 0.09	4.60 ± 0.50	5	19	123
White-lined sphinx moth	Hyles lineata	1.55 ± 0.28	3.87 ± 0.66	1.02 ± 0.17	3.10 ± 0.20	6	31	174
Snowberry clearwing moth	Hemaris diffinis	1.81 ± 0.12	2.72 ± 0.30	1.04 ± 0.18	2.95 ± 0.06	5	19	104
Mournful sphinx moth	Enyo lugubris	1.83 ± 0.22	3.45 ± 0.19	0.96 ± 0.11	3.67 ± 0.10	5	18	103
Nessus sphinx moth	Amphion floridensis	1.87 ± 0.22	2.4 ± 0.1	0.5 ± 0.1	2.3 ± 0.1	2	6	26
Laurel sphinx moth	Sphinx kalmiae	1.43 ± 0.29	4.0 ± 0.1	0.8 ± 0.1	0.9 ± 0.1	2	4	21
Banded sphinx moth	Eumorpha fasciatus	1.36 ± 0.14	3.85 ± .50	0.82 ± 0.1	4.3 ± 0.1	3	8	41
Lepidoptera species (larvae)	**Lepidoptera species (larvae)**							
Tobacco hornworm	Manduca sexta	1.66 ± 0.37	7.8 ± 0.3	1.3 ± 0.1	-	6	11	63
Blattodea species	**Blattodea species**							
American cockroach	Periplaneta americana	1.83 ± 0.41	3.5±0.7	1±0.2	2.7±0.3	9	27	135

This analysis of shear viscosity suggests that hemolymph dripping from the wound does not behave as a thick honey-like fluid. And the hemocytes had no time to aggregate. Therefore, the appearance of cylindrical filaments when hemolymph drips from the wound cannot be explained by the significant increase in its shear viscosity.

Thus, we hypothesized that as the first step in primary clot formation, the hemolymph has to be turned into a viscoelastic fluid.

2.3. Extensional rheology of hemolymph.

To evaluate the rheological properties of hemolymph filaments, we used the setup in Figure 1B. The wound can be probed for only a few minutes after incision. That is, the time for experiment preparation was long and when we applied the probe, no dripping occurred. Thus, the wound was partially sealed by the primary clot. Placing the probe on the wound and lifting the probe (Figure 1B), we formed the first filament connecting the ball with the wound (Figure 8A). This filament was quite stable: despite the caterpillar movements, the meniscus that formed at the filament foot slid across the drop surface and did not break (Figure 8B, C). When the wounded proleg was moved up or down, the filament stretched or contracted (Figure 8E, H). The first filament took 1–20 seconds to become thin and break up (Figure 8I, J). We call these liquid bridges 'long-lived filaments' (LLF), indicating that their lifetime is greater than 1 second. These long-lived filaments sometimes developed single or multiple droplets, which remained on the filament until its breakup or moved to the ends. The droplet that moved to the wound was re-absorbed by the wound, and the droplet that moved to the ball was re-absorbed by the film on the ball.

When the probe was applied for the second time, the filament was less stable and broke in less than 1 second (Figure 9). We called these filaments 'short-lived filaments' (SLF). They behaved like those dripping from the wound (Figure 3).

After the second trial, when the probe touched the wound and was then raised, the liquid bridges broke in less than 10 ms, following the breakup stages in Figure 2. These observations suggested that hemolymph behaved as a simple low-viscosity Newtonian liquid like water that does not form cylindrical filaments[29, 30]. (See an example in Supplementary material, Video S2).

Using short-lived filaments as representatives of those dripping from the wound and assuming that they would reflect the properties of the dripping filaments, we characterized their rheological properties. The rheological properties of hemolymph were evaluated by tracking the radius of the short-lived filaments with time. Analyzing the kinetics of liquid-bridge thinning, we discovered that the bridge radius followed the exponential law:

$$R = R_0 \exp\left(\frac{-t}{3\theta}\right) \quad (1)$$

with relaxation time θ. These kinetics are typically expected for a viscoelastic fluid following the Oldroyd-B constitutive equation [32, 41-45]. The Oldroyd-B fluid is characterized by two constants: its shear viscosity η and relaxation time θ. The measured relaxation time of this viscoelastic hemolymph ranges between 2 and 4 milliseconds (Figure 10). Inspection of Figure 3 confirms that this estimate of relaxation time is reasonable. Specifically, three filaments were filmed after the drop fell to the substrate and the filaments were thinning in the same manner as those in Figure 9 due to capillary action. The analysis of those filaments gave the average relaxation time of $\theta \sim 5\ ms$. Thus, filament stabilization in the dripping hemolymph can be explained by its viscoelasticity[46, 47].

To evaluate the cause of distinct kinetics of the SLF and LLF thinning, we turned to the structural analysis of their composition. When we probed the wound with the ball in the first 3 minutes, long-lived filaments were formed 13 times, short-lived filaments were formed 18 times, and 22 trials produced no filaments. For wounds older than 8 minutes, we observed a long-lived filament only once; short-lived filaments were seen 11 times, and 52 trials produced no filaments. The long-lived filaments did not necessarily follow the Oldroyd-B model or have a broad dispersion of the relaxation times ranging from

milliseconds to seconds. This scattering of the materials parameter led us to hypothesize that because of the caterpillar movements, the ball might have probed hemolymph from different depths of ball immersion. We suspected that the ball making the long-lived filaments might have probed the primary clot together with the layer of hemocytes covering the wound surface. Sometimes, one can see the flowing hemocytes inside the LLF, Supplementary video S2.

By collecting long-lived filaments on a glass slide and studying them using phase-contrast microscopy, we discovered filamentous cores made of polymeric filaments with embedded hemocytes (Figure 10B–D). These filaments were long and bundled, even without hemocytes. When a long-lived filament was broken at one end, some droplets sometimes remained on a dried filament and formed a crusted surface while the drop interior remained full of liquid hemolymph (Figure 10E).

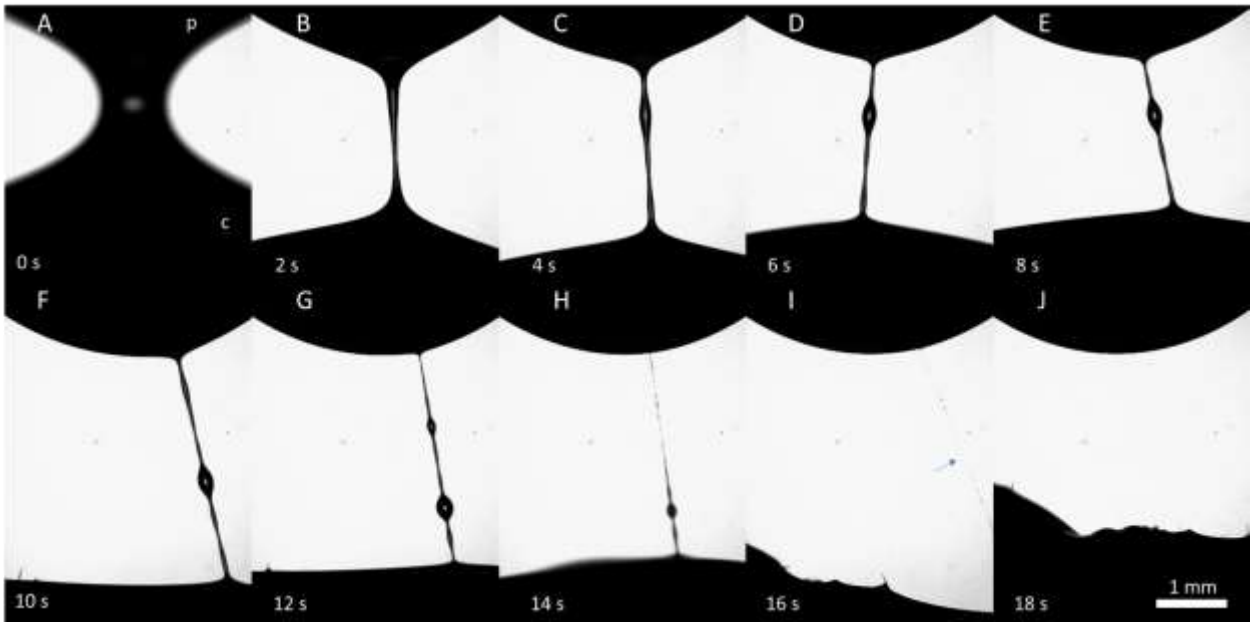

These observations confirm that the LLFs contain primary clots, and hence, their thinning kinetics is controlled by the deformations and flow of the highly inhomogeneous composite structure of primary clots. The more mature the primary clot is, the slimier it is, and the slower the filament breaks up.

Figure 8. A series of frames illustrating features of the formation and breakup of a long-lived filament (LLF). The filament formed between a stainless steel probe (p) at the top and a wound of the Manduca sexta caterpillar (c) at the bottom. The camera was focused on the filament and the wound is not visible. The caterpillar constantly moved, causing the filament to move.

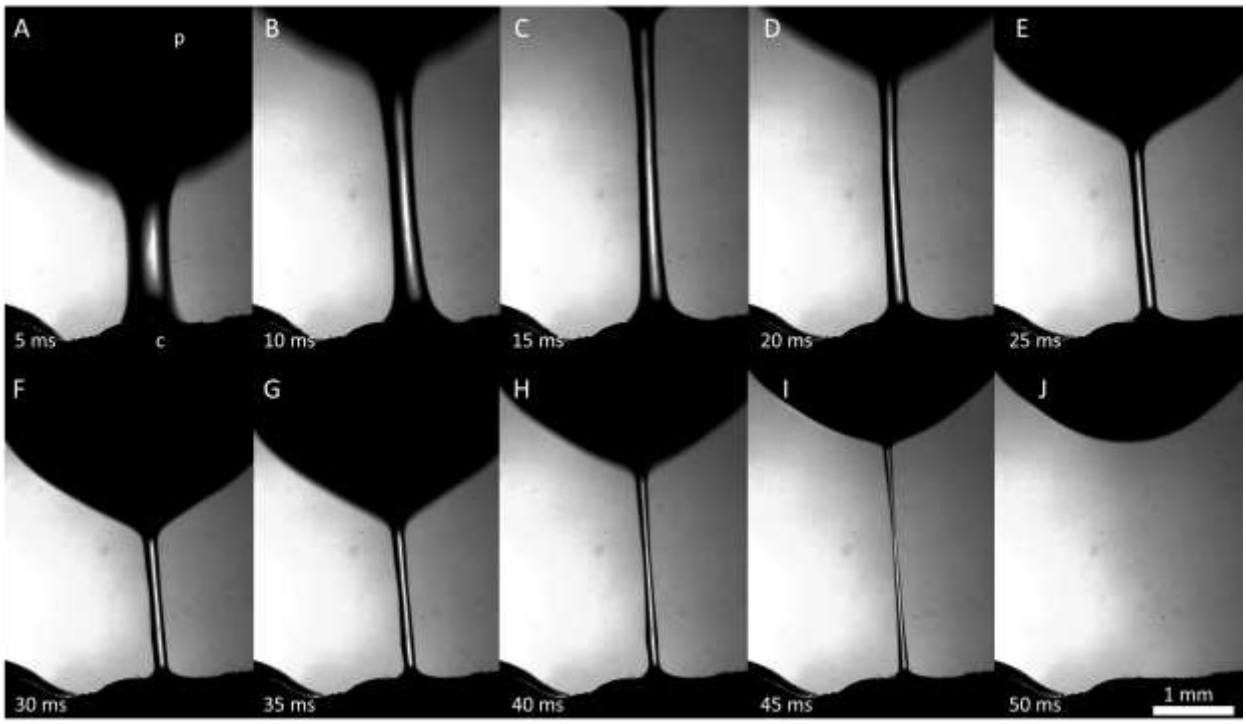

Figure 9. A series of frames illustrating features of the formation and breakup of a short-lived filament (SLF); (p) is a stainless-steel probe and (c) is the wound of the Manduca sexta caterpillar. It takes about 45 ms for the SLF to break up and disappear.

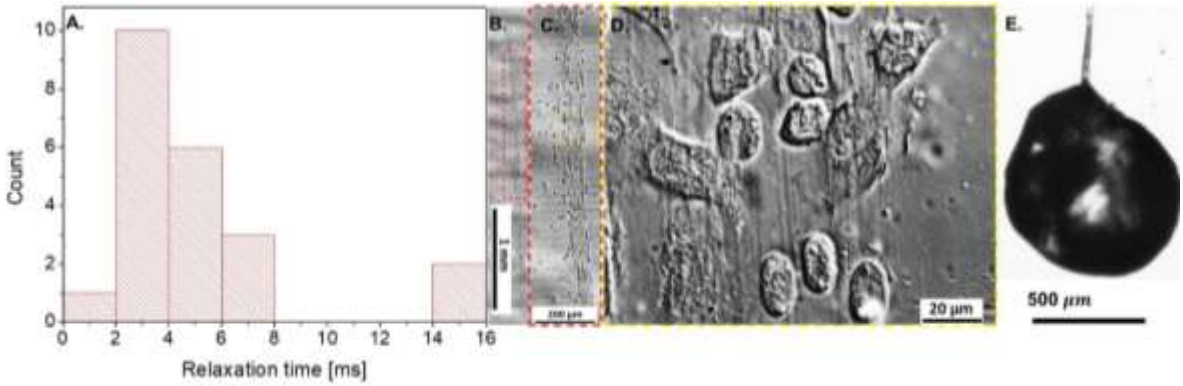

***Figure 10**. (A) The relaxation time θ measured for 4 Manduca sexta caterpillars with 22 liquid bridges. The short-lived filaments appeared viscoelastic and the majority had relaxation time θ between 2 and 4 milliseconds. (B–D) Phase-contrast optical microscopy of the filamentous core in long-lived filaments. The boxed region in B is magnified in C and the box in C is magnified in D. The core of the long-lived filament consisted of a network of micron- and submicron-diameter filaments with embedded hemocytes. (E) The hanging drop remained on a long-lived filament after making this filament from the pool of hemolymph as in Figure 1C. The lower filament connecting the drop with the hemolymph pool was naturally broken following the scenario in Figure 8, but the weight of the remaining liquid drop was balanced by the stresses in the supporting filament. Water naturally evaporated from the filament while the surface of the drop formed a crust that contained the interior as liquid hemolymph.*

2.4. Clotting starts with the interfaces.

To further investigate the phenomenon of crust formation, we examined the behavior of hemolymph drops using X-ray micro-CT and SEM imaging. X-ray imaging is attractive because it distinguishes the structure of multiphase and multicomponent materials[48, 49]. Before submitting the hemolymph drop for X-ray imaging, we rapidly froze the drop on a metal substrate and slowly sublimated the water (explained in Materials & Methods). Then, a freeze-dried drop was imaged with an X-ray microscope (Bruker Skyscan 1176). The images were reconstructed (Figure 11A, B), and we schematically show how the parallel and perpendicular cross-sections to the substrate were taken (Figure 11C). These images illustrate the density distribution of primary aggregates or clots through the drop thickness. The material closer to the air/hemolymph and hemolymph/substrate interfaces had greater density.

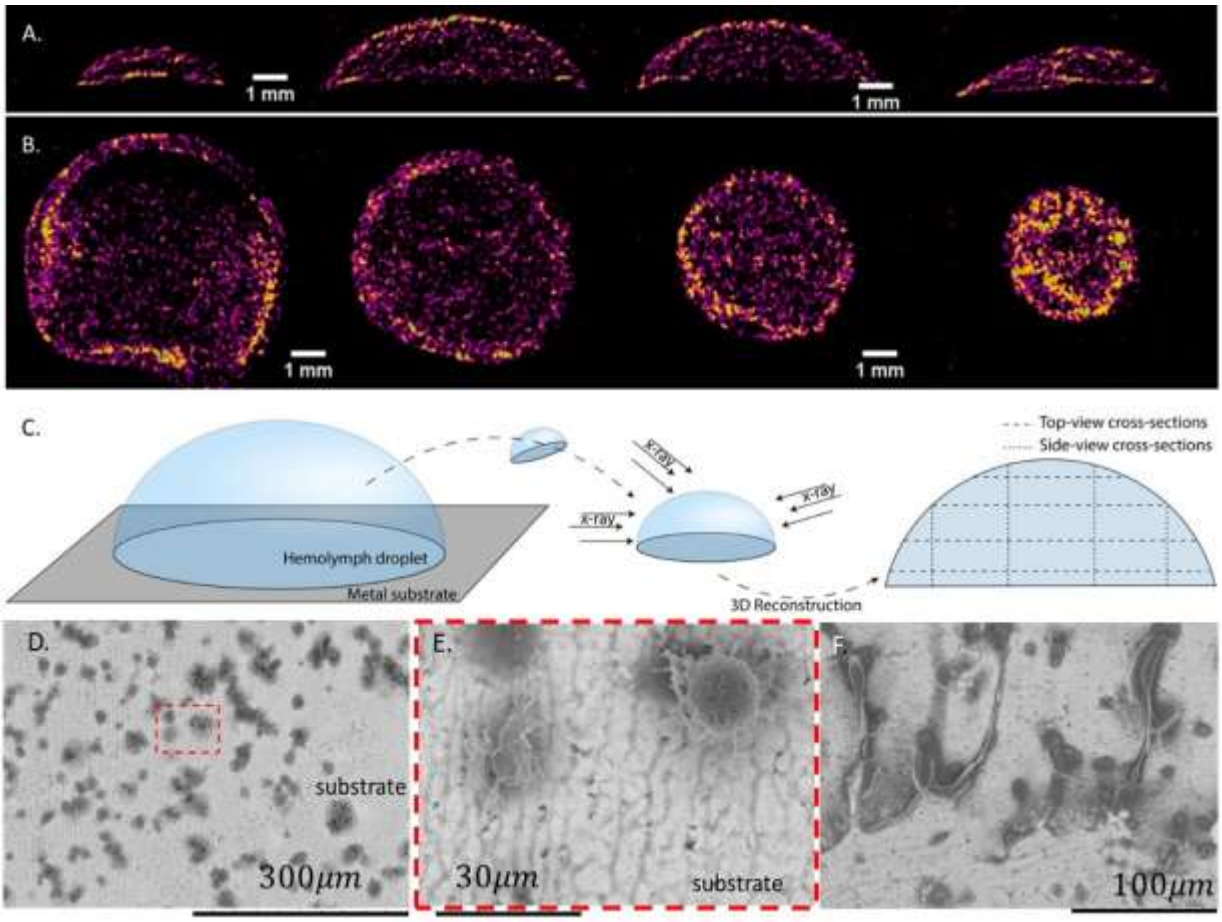

Figure 11. MicroCT scans of a freeze-dried hemolymph drop. Yellow represents a high-density material and purple represents a low-density material. (A) A series of drop cross-sections was taken perpendicular to the substrate, specified in C. The cross-sectional area increased from the drop edge to the center. (B) A series of drop cross-sections was taken parallel to the substrate, specified in C. The cross-sectional area decreased from the substrate to the droplet top. The interfacial layer of hemolymph appears to have a high-density material. (C) A diagram depicting the sample preparation procedure and the locations of the four parallel and perpendicular sections. (D) SEM micrographs of hemolymph residues attached to the substrate. Small dark spots form either chain-like or solitary aggregates. (E) Solitary aggregates appeared in the framed area in D. (E) Filamentary residues sticking out from the aggregate are also common for larger aggregates.

To evaluate the microstructure of this interfacial layer, the frozen drop was broken and removed from the substrate. The remaining material that adhered to the substrate was examined with scanning

electron microscopy. Figure 11D–F shows residues on the substrate from the droplet sitting on it for longer than 20 minutes before freezing. Chain-like aggregates are seen attached to the substrate. These aggregates are much larger than the individual hemocytes, suggesting that the hemocytes had already been assembled into chain-like primary clots. The possible building blocks of these chain-like aggregates are shown in Figure 11E, where solitary aggregates of about 30 μm in diameter were found. Filamentary residues covered the boundaries of larger primary clots (Figure 11F). These filaments were like those described in Ref.[50, 51]. No visible filaments were found in the droplets incubated for less than 20 minutes.

All these findings favor the hypothesis that in larval Lepidoptera, the primary clots first nucleate at the interfaces and form a crust-like shell preventing water evaporation. The shell propagates inwardly to occupy the entire drop.

2.5. Interfacial interactions between hemocytes in hemocyte-rich hemolymph.

Closer to the surface, hemocytes interact one with another. It has long been hypothesized that some hemocytes extrude thread-like projections (i.e., pseudopodia) in response to foreign surfaces; then other hemocytes adhere to the formed network [1, 10]. This hypothesis implicitly assumes that hemocyte density is high enough to allow connection of two neighboring hemocytes by pseudopodia [1, 52].

We investigated this hypothesis by observing hemocyte behavior in the droplets released from the wound. Within about three minutes from the moment of drop formation, the hemocytes from larvae of *M. sexta* began adhering to each other. When a magnetic nanorod was introduced to the drop, the pseudopodia anchored the nanorods to the hemocyte aggregates; nanorods never broke hemocytes. In contrast to the free nanorods, the nanorods that attached to hemocyte aggregates did not make full revolutions [13]. Instead, they beat in response to the applied rotating field around an equilibrium direction, revealing hidden interconnections between hemocytes (Supplementary video S3). During these oscillations, the surrounding cells moved in unison with the nanorod. Thus, the hemocytes with the attached nanorods mechanically communicated with neighboring hemocytes that were not visibly connected to one another. A hidden biopolymer network provides a far-field reaction to a local perturbation, engaging hemocytes in the movement. This local perturbation of an oscillating nanorod propagates through an area with a radius of ~ 5–8 nanorod lengths from the probing nanorod (Figure 12.) The analysis of nanorod oscillations in these aggregates suggested that the aggregates with a hidden network connecting them behaved as a viscoelastic material with temporary cross-links[13], as described by the Green-Tobolsky theory of gels[53].

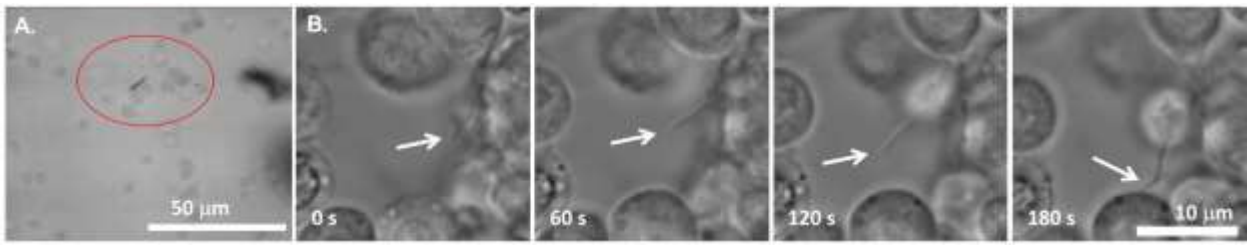

Figure 12. A) Image of a nanorod surrounded by a network of cells. The encircled hemocytes are engaged in the movement of the nanorod. As the nanorod attempts to rotate, the hemocytes inside a circled aggregate move together. The hemocytes outside the circle do not respond to the motion of the nanoprobe, indicating that the hemocytes form an aggregate shielding a foreign object

from the surrounding hemocytes. B) Phase-contrast image of a growing pseudopodium (arrows). After ~ 180 s, the two hemocytes become connected through a pseudopodial bridge. (Adapted from Ref. [13]).

The high density of hemocytes can be expected only in the neighborhood of wounded tissue; otherwise, the hemocyte density in a healthy caterpillar is insufficient for hemocyte bridging. We illustrated this statement by showing that after ~ 3 minutes of being close to one another in a large population of hemocytes, only two of them became bridged by a pseudopodium; the other hemocytes remained mobile (Figure 12B).

An illustrative scenario of hemocytes gathering in a primary clot during the first 10 minutes of hemolymph coagulation is presented in Figure 13 [13]. A pseudopodium extends from the originating mother hemocyte, further stretches, and bends on its way, targeting another hemocyte to which it adheres. The pseudopodium functions as a hydraulic spring: on its way to finding the target, it stretches the constituent material. After contact, the pseudopodium tends to spread along the hemocyte surface. The tension generated in the hemocyte during stretching tends to relax, squeezing the constituent material back to the mother hemocyte and dragging the targeted hemocyte with it. As the pseudopodium contracts toward the mother hemocyte, it may encounter another hemocyte, attach to it, and bring it to the mother hemocyte. The process repeats and the aggregates grow larger and change their shape, leading to formation of a primary clot[1, 10, 13].

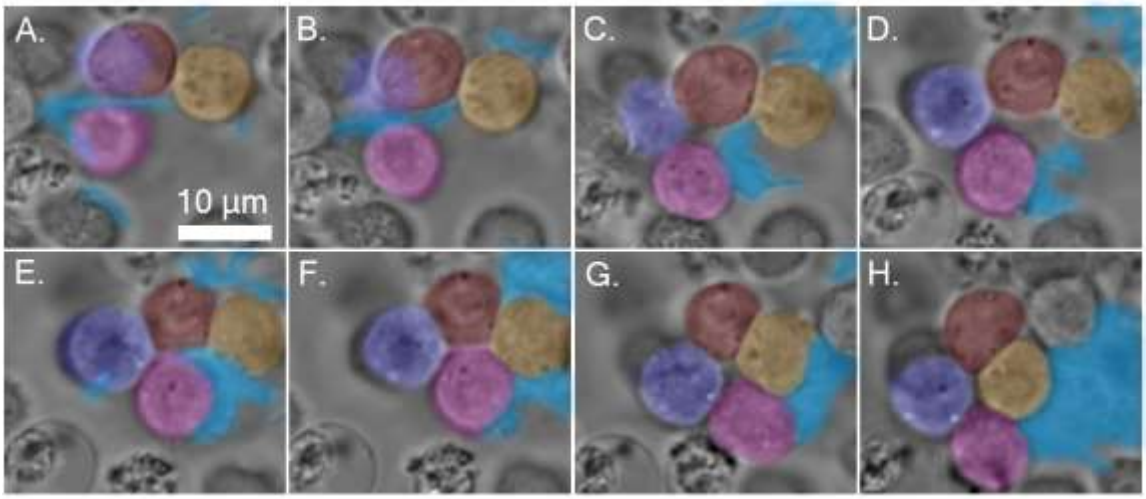

Figure 13. A gallery of time-lapse frames, depicting a 4-hemocyte aggregate in a primary clot of hemolymph of a larva of Manduca sexta. The pseudopodia are formed by hemocytes first deforming the interface in the finger-like extensions. Each extension could deform and propagate over long distances searching for a target. The hemocytes are artificially colored in red, yellow, purple, and pink and the aggregate-involved pseudopodia are in blue. (A) Initially, the red and yellow hemocytes are weakly touching, and the pink hemocyte is free near extending pseudopodia. (B, C) With time, the interface between the red and yellow hemocytes increases, while the pseudopodium attaches to the pink hemocyte and drags it to the right. (D) The purple hemocyte, which is attached to both red and pink hemocytes, comes into focus, while the pseudopodium continues to drag the pink hemocyte to the right. (E) The red/purple and the pink/purple interfaces grow and the pink hemocyte, which is half-engulfed in pseudopodia, first touches the red hemocyte. (F) The pink hemocyte disconnects from the pseudopodia and attaches to the red and yellow hemocytes. (G) The red and pink hemocytes disconnect and the 4-hemocyte aggregate forms a hole at the center. (H) The purple and yellow hemocytes form an interface and the four hemocytes remain in this configuration until the end of observation. (Images were extracted from the video in Ref. [13]).

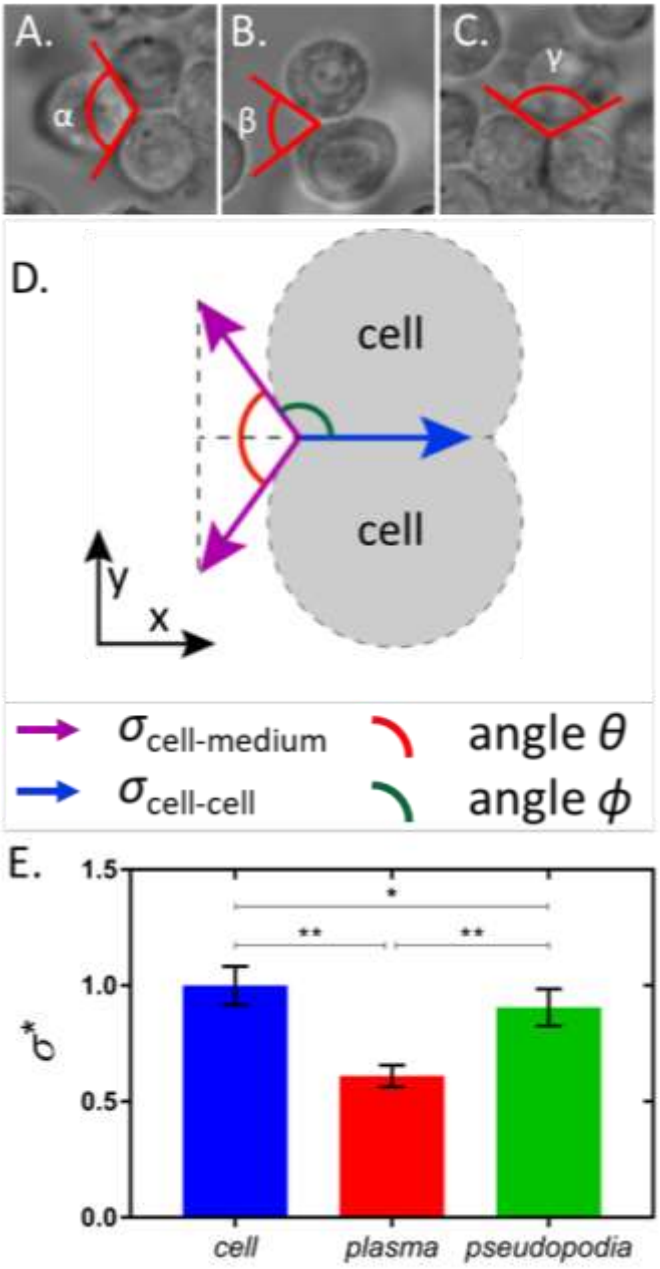

The mechanism of hemocyte adhesion by pseudopodia can be understood from the analysis of the strength of adhesion bonds between hemocytes in the aggregate. The interfacial tensions and associated interfacial energies of films separating the adjacent hemocytes offer quantitative metrics for analysis of aggregation phenomena (Figure 14). These interfacial tensions control the opening angle θ introduced as the angle of the wedge that the two hemocyte interfaces make at the contact (Figure 14D). We distinguish the wedges filled with different media of interest. At least three types of wedges could be formed by the two hemocyte interfaces in the primary aggregate when hemocytes contacted each other (Figure 14 A–C). When the wedge is filled with the hemocyte interior and two interfaces in the wedge separate three different hemocytes, we call the wedge angle θ = α. When the wedge is filled with plasma and two interfaces separate hemocytes from plasma, we call the wedge angle θ = β. When the wedge is filled with pseudopodia and two interfaces separate hemocytes from pseudopodia, we call the wedge angle θ = γ.

*Figure 14. The opening angle of the wedge formed by two hemocyte interfaces in different environments: (A) when three hemocytes reside in a primary clot and their interfaces form a wedge of angle α filled with the hemocyte interior; (B) when two hemocyte interfaces form a wedge of angle β filled with plasma; (C) when two hemocyte interfaces form a wedge of angle γ filled with pseudopodia. (D) Free body diagram for the interfacial tensions acting at the vertex. The associated tensions, the opening angle θ, and the complementary angle ϕ are shown in different colors. (E) Bar graph of relative interfacial energies calculated using equation (3) where asterisks correspond as follows: * $p < 0.05$. ** $p < 0.0001$. The number of measurements for each scenario is n_α=12, n_β = 14, and n_γ = 7.*

We introduce the interfacial tension $\vec{\sigma}_{cell-cell}$ between two identical hemocytes sharing a common interface and the interfacial tension $\vec{\sigma}_{cell-medium}$ separating a hemocyte from the surrounding medium (Figure 14D). These vectors are parallel to interfaces and perpendicular to the contact line that runs perpendicular to the figure. In the introduced Cartesian system of coordinates, the x-axis is parallel to vector $\vec{\sigma}_{cell-cell}$. Setting up a free-body-diagram at the vertex where three interfaces meet (Figure 14 D), we have

$$\vec{\sigma}_{cell-medium} + \vec{\sigma}_{cell-medium} + \vec{\sigma}_{cell-cell} = 0 \quad (2)$$

Balancing the x-components of forces, we obtain

$$\sigma_{cell-medium} \cos\left(\frac{\theta}{2}\right) + \sigma_{cell-medium} \cos\left(\frac{\theta}{2}\right) = \sigma_{cell-cell} \quad (3)$$

The measured angle α = 120 ± 5° is close to *α* = 120°, as predicted by the Plateau law [54] for the bubble and droplet aggregates with the same interfacial tension $\sigma_{cell-cell}$. Therefore, we conclude that these aggregates are formed by the same hemocytes with the same interfacial energy $\sigma_{cell-cell}$. This interfacial energy $\sigma_{cell-cell}$ is assigned for the interfacial energy of hemocytes in the preliminary clot. The relative change of the interfacial energy referenced to $\sigma_{cell-cell}$ is introduced as

$$\sigma^*_{medium} = \sigma_{cell-medium} \Big/ \sigma_{cell-cell} = \left[2\cos\left(\frac{\theta}{2}\right)\right]^{-1}, \quad (4)$$

Using the measured angles α = 120 ± 5°, β = 70 ± 11°, and γ = 113 ± 6°, the relative interfacial energies of hemocytes in a primary clot (σ^*_{cell}), the two-hemocyte aggregate in plasma (σ^*_{plasma}), and the two-hemocyte aggregate in pseudopodia ($\sigma^*_{pseudopodia}$) were calculated as σ^*_{cell} = 1.00 ± 0.08, σ^*_{plasma} = 0.61 ± 0.05, and $\sigma^*_{pseudopodia}$ = 0.91 ± 0.08 (Figure E). These estimates confirm that pseudopodia form a landing bed for incoming hemocytes and only ~ 10% of extra bonds are required to lock the hemocyte in the aggregate.

This analysis emphasizes the importance of interfacial forces in gathering and holding hemocytes together during the development of primary clots.

3. DISCUSSION AND CONSCLUSIONS.

In recent years, the fruitful analogy between the cell aggregates of developing tissues and liquids with a viscoelastic rheology has offered new perspectives in biological soft matter[55-61]. Although the mainstream research in this direction is focused on vertebrate and human blood, little is known about materials properties of insect blood. We, therefore, investigated the hemolymph clotting phenomena using materials science approaches. The main question that we asked was: “What are the materials determinants of fast wound sealing in insects?” By evaluating rheological properties of hemolymph over short periods of time, we investigated the mechanisms leading to arrest of bleeding and to nucleation and formation of primary clots in insects with hemocyte-rich hemolymph.

Our experiments were triggered by observations of hemolymph extracted directly from a wound. When a metal pin is dipped in a hemolymph drop with primary clots and then immediately pulled back, one observes a liquid filament bridging the droplet surface with the pin. The hemolymph filament does not break as quickly as a water bridge formed with the same pin drawn from a water droplet. This feature of hemolymph stringing [13, 19, 27, 62] is the first indication of clotting. It can be used for screening different clot inhibitors or promoters, as demonstrated with hemolymph of fruit fly larvae (*Drosophila melanogaster*) [28, 63]. The authors of Refs. [28, 63] studied the effect of the protein phenoloxidase (PO) on clot tenacity by measuring the maximum pull-out length of the filament in the hemolymph droplets with and without PO. This protein is thought to facilitate cross-linking and hardening of the primary clot. One would expect that the greater the PO concentration, the harder the clot and the shorter the pull-out

length of the filament before it breaks. This prediction is correct [28, 63]. Although these observations are useful, no quantitative data on materials properties of hemolymph have been provided. The most challenging biological question regarding the mechanism of fast wound sealing remained enigmatic.

We found that larvae of *Manduca sexta*, which have hemocyte-rich hemolymph, stopped bleeding after 60–90 seconds. At this time scale, hemolymph viscosity is low (Table 1), and high-speed videography is needed to film filament breakup (Figures 2, 3, 9). The appearance of a long cylindrical filament in the dripping hemolymph points to its possible viscoelasticity [46, 64]. Many low-shear viscosity biofluids demonstrate viscoelasticity[45, 65]. Hemolymph could behave like saliva dripping from a dog's mouth with water-level low shear viscosity, yet capable of producing long filaments. Making an aqueous fluid elastic allows an animal to stabilize the flow of blood through the circulatory system or prevent the breakup of liquid bodies, as in the case of dripping hemolymph.

The kinetics of breakup of a cylindrical filament decreasing its radius due to capillary action allows one to evaluate the rheological properties of fluids and distinguish the specifics of viscoelastic non-Newtonian behavior of the material[32, 41, 66]. We, therefore, analyzed the kinetics of filament breakup and observed that before the arrest of bleeding, the hemolymph became viscoelastic with the relaxation time $2\ ms$ (Figure 10 A).

Knowing the relaxation time and the shear viscosity (Table 1), $\eta = 1.66\ mPa \cdot s$, the elastic modulus $G \sim \eta/\theta$ of the elastic additives in the filament can be estimated as $G \sim 2\ Pa$. At least two possible elastic contributors are present in hemolymph: biopolymers and hemocytes. Collecting the short-lived filaments of interest during bleeding and analyzing them under the microscope, we found no hemocytes. Therefore, the hemolymph elasticity might come only from biopolymers in the hemolymph. Assuming that biopolymers form a weak network, and using the rubber elasticity theory $G \sim \nu k_B T$ [37, 46], where k_B is the Boltzmann constant and T is the absolute temperature, we can estimate the density ν of crosslinks. At room temperature, $k_B T \approx 10^{-21} J$, the 2 Pa network should contain $\nu \sim 10^{21}\ m^{-3} = 1000 \mu m^{-3}$; that is, a single crosslink is expected per cube with 100 nm sides. Thus, the distance between crosslinks is greater than the typical radius of gyration of proteins, suggesting that to self-assemble into bundles, proteins should unfold from their globular state [67].

Typically, hemolymph plasma contains from 0.01 to 0.1 % w/w of different proteins, some with large molecular weight, up to 500 kDa[68]. Geng and Dunn [50, 51] hypothesized that an insect's immune response makes some fibrous proteins self-assemble into a network. Among a variety of insect proteins, lipoproteins are known for their ability to self-assemble in chain-like aggregates of more complex biopolymer subunits [6, 7, 18-25, 69]. Many other fibrous proteins can do the same[14, 15]. Even a minute concentration of chains makes the fluid elastic. For example, even dilute polymer solutions where polymeric coils are far apart can stabilize liquid bridges and jets and turn them into constant-radius cylinders[47, 70-72]. Therefore, making hemolymph viscoelastic is critical to stopping the bleeding.

Even after the arrest of bleeding, wound closure must be fast to prevent water and solute loss, maintain hydrostatic pressure, and form a barrier to infection. At this step, the viscoelasticity of low-viscosity hemolymph does not help much, and the insect develops a new strategy by forming a clot that spreads to form a stiff wound seal. Hemocyte-rich hemolymph contains adhesive and non-adhesive hemocytes[1, 73, 74]. One scenario of clot nucleation assumes that the adhesive cells aggregate at the wound surface or any other surface [2, 55, 57, 75-78] and are involved in wound healing, phagocytosis [1, 3, 27, 73, 74, 79-82], and the regrowth of epidermal cells [52, 83-86]. In this scenario, primary clots are formed at the wound surface or any other foreign surface. We showed that in larvae of *M. sexta*, primary

clots are formed at the interfaces (Figure 11) and propagate from the damaged surface toward the hemolymph interior. This scenario has been observed for other insects [1, 2, 22, 27].

Hemocytes spread over and embed in a fibrous network of primary clots, as illustrated by analysis of the core of long-lived filaments (Figure 10). The importance of interfacial forces in gathering and holding hemocytes together during the development of primary clots is illustrated in Figures 12 and 13 and by the theoretical analysis in Section 2.5.

The Ni-nanorod experiments and phase-contrast imaging of these primary clots showed that fibrous connectors are essential to hold hemocytes inside the aggregate and make connections between the aggregates. We showed that about 90% of the adhesion energy between hemocytes comes from the surrounding fibrous bed. To permanently lock hemocytes in the aggregate, only ~ 10% needs to be added to the adhesion energy. These additional bonds are formed later in clot development during consolidation of the aggregates [13].

In summary, we observed that insects with hemocyte-rich hemolymph develop a two-step strategy to form clots. In the first step, Newtonian plasma of hemolymph turns into a non-Newtonian viscoelastic fluid remaining at very low viscosity. This transformation allows retraction of the dripping hemolymph to the wound. At the second step, primary clots nucleate and start forming a crust at the air-hemolymph and hemolymph-substrate interfaces. The clots propagate from the interface toward the droplet center.

Given the adaptive value of viscous to viscoelastic fluid conversion, we expect this physical phenomenon to be widespread in insects, as well as other organisms, with hemocyte-rich hemolymph. In addition to insects, for example, hemocyte-rich fluids are present in some molluscs (e.g., snails), where they promote wound healing [87]. As hemocyte density changes with age and infection level in some insects[88], we also expect the physical behavior of the hemolymph to change. Intriguing experimental subjects include insects that partition hemocyte-rich and hemocyte-poor hemolymph in the same body. The larvae of at least some mosquito species, for instance, are hemocyte-rich at specific body sites, such as the openings into the heart, where they rapidly mobilize to fight infection[89].

The period from initiation of the immune cascade reaction to the first microscopically visual detection of a rheological response of hemolymph remains the unquantified bridge between molecular biology and materials science. Since the last century [78], biologists have known that vertebrate red blood cells can initiate an immune cascade reaction in hemolymph of insects. The materials manifestation of viscous to viscoelastic conversion of insect hemolymph in a few seconds is attractive for biomedical applications. We hope that our findings will trigger the interest of biochemists and molecular biologists to design fast-working thickeners for vertebrate blood including human blood.

Materials and methods

Larval maintenance

Larvae of *M. sexta* were obtained from Carolina Biological Supply (https://www.carolina.com) or reared in-house on food from Great Lakes Hornworms (https://www.greatlakeshornworm.com/), with some feeding *ad libitum* on hornworm food from Carolina Biological Supply. Deposited eggs were from adults that emerged in a net enclosure (ca. 27°C and relative humidity ca. 65%). Rearing containers were wide-mouth 1-liter glass jars with strips (ca. 3x15 cm) of plastic gutter guard (Frost King Model VX620) as a climbing substrate and food support. Larvae were kept at controlled room temperature (about 25°C) and 24 h artificial light. To provide gas exchange, the jar lids were replaced with aluminum window screens. Food (ca. 10 ml) was added in the first three instars as needed. In later instars, larvae were removed from jars and placed in clean jars with more food added as needed. The number of larvae per

jar was reduced as they grew, with 10 or fewer last instars per jar. Larvae entering pre-pupation (i.e., those with a more yellowish thorax, no longer eating, and in a wandering phase) were not used as a source for hemolymph.

Hemolymph extraction

Larvae of *Manduca sexta* 1–2 days before pre-pupation and weighing more than 8.5 g were used. The caterpillars were washed free of contaminants with DI water and dried with a paper towel. To minimize movement of larvae, they were placed in specially designed containers (Figure 1) that gripped the larva along the length of the body while exposing the second and third prolegs. Hemolymph was extracted via a 1–2 mm incision made by a razor blade in the third proleg. Hemolymph exiting the wound was collected on a glass slide or probed directly on the body. All experiments were conducted at 20–22°C.

Phase-contrast imaging

To investigate the LLF structure, a liquid bridge was created between a hemolymph drop and the metal ball (Fig. 1C). A glass slide was placed next to the ball perpendicularly to the drop surface so that the slide touched the ball side. Pulling the ball parallel to the glass slide above the slide edge stretched the liquid bridge and formed a filament. By moving the ball with the filament toward the glass surface, we deposited the filament on the slide. The deposited filament was covered with a cover slip to prevent evaporation during phase-contrast imaging.

To study cell aggregation, drops of blood were placed under an inverted transmitted-light phase-enhanced microscope (Nikon Eclipse Ti; 40X Oil Objective, S Fluor, NA=1.30, DIC H/N2; Photometrics CoolSnap HQ2 camera, 272 ms exposure, time interval=1 sec) and cell behavior was recorded. Cellular aggregation during the first 10 minutes of coagulation was observed under high magnification.

X-ray microCT & SEM imaging

A drop of hemolymph was rapidly frozen on a metal block in liquid nitrogen, freeze-dried under vacuum, detached from the metal block, mounted on a low-density Styrofoam block, and imaged with X-ray microCT (Bruker Skyscan 1176). The image was digitally reconstructed, and the cross-sections were studied. The methodology can be summarized as follows. An X-ray source in tandem with a detector was rotated around the sample and projection images of the sample were taken. The images were digitally reconstructed into a three-dimensional structure. The cross-sections of the three-dimensional structure could then be visualized. The resolution of the instrument was 9 µm per pixel, which was inadequate to observe the internal structure of the freeze-dried clots but was sufficient to determine the internal distribution of the material density.

Magnetic Rotational Spectroscopy

Nickel nanorods of $d\sim 200\,nm - 400\,nm$ diameter and $L_0\sim 7\,\mu m - 13\,\mu m$ length, with remanent magnetization of $M_r = 224$ kA/m[41], were dispersed in methanol by sonication. A droplet of the nanorod-methanol suspension was placed on a glass slide and allowed to dry at $23 \pm 1\,^0$C and $50 \pm 20\%$ humidity. Hemolymph was placed on the dried nanorod-methanol residue and stirred with a glass rod to disperse the nanorods. The hemolymph droplets were directly exposed to air (21–23 ^{o}C). To eliminate any effects of the hemolymph-substrate and hemolymph-air interfaces on viscosity, only nanorods inside the drop ($6\,\mu m$ below the air-hemolymph interface and $\sim 6\,\mu m$ above the substrate) were used. The nanorod rotation was filmed and the videos were processed using Labview and MatLab algorithms as explained in Refs.[27,28][35].

Analysis of filament rheology

The SLF & LLF breakup was filmed with an IDT Technologies MotionProX3 camera at 200–900 fps with 512–640 pixel resolution and Grasshopper Point Grey camera at 100–140 fps with 1920–1200 pixel resolution. The time dependence of the filament radius was obtained with a specially developed LabVIEW Vision Development Module that allowed us to extract and analyze the profile of the liquid bridge for each frame of the videos[90, 91]. The module used IMAQ Extract Contour algorithm to provide the filament profile. Then the radius of the cylindrical neck of the filament was fit by eq.(1) and the goodness of fit was evaluated as discussed in Refs. [90, 91]. The procedure was repeated for each filament, and the average relaxation time for the series was reported.

The study of the LLF hemolymph puddles from 10 caterpillars were tested using the setup in Fig. 1 C. The method required roughly 1.0–1.5 minutes to collect hemolymph from the bleeding caterpillar and prepare the experimental setup. Liquid bridges were formed from the same $5mm\ x\ 5\ mm$ area of the central spot of the puddles.

Acknowledgements. We thank Guzeliya Korneva and Bryan Wiggers for helping with the optical imaging and characterization of hemolymph properties, and Ahva Zadeh for helping collect the MRS data on the hemolymph of cockroaches.

Funding. This work was partially supported by NSF grant IOS 2014664, by Clemson University Creative Inquiry project to KGK and by SC BioCRAFT facilities supported by the National Institute of General Medical Sciences (NIGMS) of the National Institutes of Health under award number P30GM131959 through the Voucher Program to KGK. The work of PHA was also partially supported by the NIFA/USDA, under project number SC-1700527, with Technical Contribution No. 7237 of the Clemson University Experiment Station. The work of PA was partly supported by NASA through the SC Space Grant Consortium Graduate Assistantship, NASA Grant: NNX15AL49H.

Bibliography

1. Salt GW. The cellular defence reactions of insects. Cambridge Cambridge University Press; 1970.
2. Wigglesworth VB. Hemocytes and growth in insects. In: Gupta AP, editor. Insect hemocytes: development, forms, functions, and techniques. Cambridge, UK: Cambridge University Press; 1979. p. 303-18.
3. Gillespie JP, Kanost MR, Trenczek T. Biological mediators of insect immunity. Annual Review of Entomology. 1997;42:611-43. doi: 10.1146/annurev.ento.42.1.611. PubMed PMID: WOS:A1997WD49500025.
4. Theopold U, Li D, Fabbri M, Scherfer C, Schmidt O. The coagulation of insect hemolymph. Cellular and Molecular Life Sciences. 2002;59:363-72. doi: 10.1007/s00018-002-8428-4. PubMed PMID: 11915949.
5. Strand MR. The insect cellular immune response. Insect Science. 2008;15(1):1-14. doi: 10.1111/j.1744-7917.2008.00183.x. PubMed PMID: WOS:000252587700001.
6. Dushay MS. Insect hemolymph clotting. Cellular and Molecular Life Sciences. 2009;66:2643-50. doi: 10.1007/s00018-009-0036-0. PubMed PMID: 19418022.
7. Jiang H, Vilcinskas A, Kanost MR. Immunity in Lepidopteran insects. In: Soderhall K, editor. Invertebrate Immunity. Advances in Experimental Medicine and Biology. 708. Berlin: Springer-Verlag Berlin; 2010. p. 181-204.

8. Hillyer JF, Strand MR. Mosquito hemocyte-mediated immune responses. Current Opinion in Insect Science. 2014;3:14-21. doi: 10.1016/j.cois.2014.07.002. PubMed PMID: WOS:000209578700004.
9. Eleftherianos I, Heryanto C, Bassal T, Zhang W, Tettamanti G, Mohamed A. Haemocyte-mediated immunity in insects: Cells, processes and associated components in the fight against pathogens and parasites. Immunology. 2021;164(3):401-32. doi: 10.1111/imm.13390. PubMed PMID: WOS:000679933500001.
10. Gregoire C. Hemolymph coagulation. In: Rockstein M, editor. The Physiology of Insecta. 5. New York: Academic Press; 1974. p. 309-60.
11. Bohn H. Hemolymph clotting in insects. In: Brehelin M, editor. Immunity in invertebrates, Cells, Molecules and Defense Reactions. Heidelberg: Springer; 1986. p. 188-207.
12. Parle E, Dirks JH, Taylor D. Bridging the gap: wound healing in insects restores mechanical strength by targeted cuticle deposition. Journal of the Royal Society Interface. 2016;13(117). doi: 10.1098/rsif.2015.0984. PubMed PMID: WOS:000378311800003.
13. Aprelev P, Bruce TF, Beard CE, Adler PH, Kornev KG. Nucleation and formation of a primary clot in insect blood. Scientific Reports. 2019;9:3451.
14. Ling SJ, Kaplan DL, Buehler MJ. Nanofibrils in nature and materials engineering. Nat Rev Mater. 2018;3(4):15. doi: 10.1038/natrevmats.2018.16. PubMed PMID: WOS:000430173500002.
15. Miserez A, Yu J, Mohammadi P. Protein-Based Biological Materials: Molecular Design and Artificial Production. Chem Rev. 2023. doi: 10.1021/acs.chemrev.2c00621. PubMed PMID: WOS:000925857700001.
16. Zdybicka-Barabas A, Cytrynska M. Apolipophorins and insects immune response. Isj-Invertebrate Survival Journal. 2013;10(1):58-68. PubMed PMID: WOS:000328155800001.
17. Hu HW, Hu QB, Weng QF, Wang JJ. Hemocytin, the special aggregation factor connecting insect hemolymph immunity, a potential target of insecticidal immunosuppresant. Pesticide Biochemistry and Physiology. 2024;198. doi: 10.1016/j.pestbp.2023.105704. PubMed PMID: WOS:001135149200001.
18. Brehelin M. Hemolymph coagulation in *Locusta-migratoria* - evidence for a functional equivalent of fibrinogen. Comp Biochem Physiol B-Biochem Mol Biol. 1979;62(4):329-34. doi: 10.1016/0305-0491(79)90098-1. PubMed PMID: WOS:A1979GS50300007.
19. Chino H, Hirayama Y, Kiyomoto Y, Downer RGH, Takahashi K. Spontaneous aggregation of locust lipophorin during hemolymph collection. Insect Biochemistry. 1987;17(1):89-97. doi: 10.1016/0020-1790(87)90148-x. PubMed PMID: WOS:A1987E892900013.
20. Mulnix AB, Dunn PE. Molecular biology of immune response. In: Goldsmith MR, Wilkins AS, editors. Molecular model systems in the Lepidoptera. Cambridge, UK: Cambridge University Press; 1995. p. 369-96.
21. Maravilla E, Le DP, Tran JJ, Chiu MH, Prenner EJ, Weers PMM. Apolipophorin III interaction with phosphatidylglycerol and lipopolysaccharide: A potential mechanism for antimicrobial activity. Chemistry and Physics of Lipids. 2020;229:10. doi: 10.1016/j.chemphyslip.2020.104909. PubMed PMID: WOS:000531098600005.
22. Theopold U, Schmidt O, Soderhall K, Dushay MS. Coagulation in arthropods: defence, wound closure and healing. Trends Immunol. 2004;25(6):289-94. doi: 10.1016/j.it.2004.03.004. PubMed PMID: WOS:000222302100004.
23. Boman HG, Hultmark D. Cell-free immunity in insects. Annu Rev Microbiol. 1987;41:103-26. doi: 10.1146/annurev.mi.41.100187.000535. PubMed PMID: WOS:A1987K194900005.
24. Coodin S, Caveney S. Lipophorin inhibits the adhesion of cockroach (*Periplaneta americana*) hemocytes *in vitro*. Journal of Insect Physiology. 1992;38(11):853-62. doi: 10.1016/0022-1910(92)90096-v. PubMed PMID: WOS:A1992JZ89400005.

25. Rahman MM, Ma G, Roberts HLS, Schmidt O. Cell-free immune reactions in insects. Journal of Insect Physiology. 2006;52(7):754-62. doi: 10.1016/j.jinsphys.2006.04.003. PubMed PMID: WOS:000239081500012.
26. Staczek S, Zdybicka-Barabas A, Mak P, Sowa-Jasilek A, Kedracka-Krok S, Jankowska U, et al. Studies on localization and protein ligands of Galleria mellonella apolipophorin III during immune response against different pathogens. Journal of Insect Physiology. 2018;105:18-27. doi: 10.1016/j.jinsphys.2017.12.009. PubMed PMID: WOS:000427218000003.
27. Gregoire CH. Blood coagulation in arthropods. V. Studies on hemolymph coagulation in 420 species of insects. Arch Biol. 1955;66((1)):103-48. PubMed PMID: BCI:BCI19563000004464.
28. Bidla G, Lindgren M, Theopold U, Dushay MS. Hemolymph coagulation and phenoloxidase in Drosophila larvae. Developmental and Comparative Immunology. 2005;29:669-79. doi: 10.1016/j.dci.2004.11.007. PubMed PMID: 15854679.
29. Eggers J. Nonlinear dynamics and breakup of free-surface flows. Rev Mod Phys. 1997;69(3):865-929. doi: 10.1103/RevModPhys.69.865. PubMed PMID: WOS:A1997XL66500009.
30. Montanero JM, Ponce-Torres A. Review on the Dynamics of Isothermal Liquid Bridges. Applied Mechanics Reviews. 2020;72(1). doi: 10.1115/1.4044467. PubMed PMID: WOS:000525416400003.
31. Chapman RF. The Insects: Structure and Function. 2013.
32. McKinley GH, Sridhar T. Filament-stretching rheometry of complex fluids. Annual Review of Fluid Mechanics. 2002;34:375-415. doi: 10.1146/annurev.fluid.34.083001.125207. PubMed PMID: WOS:000174038400017.
33. Gu Y, Kornev KG. Ferromagnetic Nanorods in Applications to Control of the In-Plane Anisotropy of Composite Films and for In Situ Characterization of the Film Rheology. Advanced Functional Materials. 2016;26(22):3796-808. doi: 10.1002/adfm.201504205. PubMed PMID: WOS:000379128700004.
34. Kornev KG, Gu Y, Aprelev P, Tokarev A. Magnetic rotational spectroscopy for probing rheology of nanoliter droplets and thin films". In: Kumar CSSR, editor. Springer book series on Characterization Tools for Nanoscience & Nanotechnology. 6. New York: SPRINGER; 2016. p. 51-83.
35. Brasovs A, Palaoro AV, Aprelev P, Beard CE, Adler PH, Kornev KG. Haemolymph viscosity in hawkmoths and its implications for hovering flight. Proc R Soc B. 2023;290:20222185. doi: https://doi.org/10.1098/rspb.2022.2185.
36. Jeffery GB. The motion of ellipsoidal particles in a viscous fluid. Proceedings of the Royal Society of London Series a-Containing Papers of a Mathematical and Physical Character. 1922;102(715):161-79. doi: 10.1098/rspa.1922.0078. PubMed PMID: WOS:000202801300004.
37. Doi M, Edwards SF. The theory of polymer dynamics. Oxford: Clarendon Press; 1988. xiii, 391 p. p.
38. Kornev KG, Neimark AV, Rozhkov AN. Physical mechanisms of foam flow in porous media. Rheology Series. 8: Elsevier; 1999. p. 1151-82.
39. Aprelev P, McKinney B, Walls C, Kornev KG. Magnetic stage with environmental control for optical microscopy and high-speed nano- and microrheology. Physics of Fluids. 2017;29(7):072001. doi: 10.1063/1.4989548. PubMed PMID: WOS:000406765200003.
40. Kenny MC, Giarra MN, Granata E, Socha JJ. How temperature influences the viscosity of hornworm hemolymph. Journal of Experimental Biology. 2018;221(21):7. doi: 10.1242/jeb.186338. PubMed PMID: WOS:000449824800016.
41. Bazilevsky AV, Entov VM, Rozhkov AN, editors. Liquid filament microrheometer and some of its applications. The Golden Jubilee Meeting of the British Society of Rheology and Third European Rheology Conference; 1990; Edinburgh, UK.
42. Bazilevskii AV, Entov VM, Rozhkov AN. Breakup of an Oldroyd liquid bridge as a method for testing the rheological properties of polymer solutions. Polymer Science Series A. 2001;43(7):716-26. PubMed PMID: WOS:000170282300008.

43. Rodd LE, Scott TP, Cooper-White JJ, McKinley GH. Capillary break-up rheometry of low-viscosity elastic fluids. Applied Rheology. 2005;15(1):12-27. doi: 10.1515/arh-2005-0001. PubMed PMID: WOS:000233116600004.
44. Kojic N, Bico J, Clasen C, McKinley GH. Ex vivo rheology of spider silk. Journal of Experimental Biology. 2006;209(21):4355-62. doi: 10.1242/jeb.02516. PubMed PMID: WOS:000242132500027.
45. Bazilevsky AV, Entov VM, Rozhkov AN. Breakup of a liquid bridge as a method of rheological testing of biological fluids. Fluid Dyn. 2011;46(4):613-22. doi: 10.1134/s0015462811040119. PubMed PMID: WOS:000294174000011.
46. Larson RG. The structure and rheology of complex fluids. Gubbins KE, editor. New York: Oxford University Press; 1999. 663 p.
47. Bazilevskii AV, Meyer JD, Rozhkov AN. Dynamics and Breakup of Pulse Microjets of Polymeric Liquids. Fluid Dyn. 2005;40(3):376-92. doi: 10.1007/s10697-005-0078-4. PubMed PMID: WOS:000207870400005.
48. Andrews JC, Meirer F, Liu YJ, Mester Z, Pianetta P. Transmission X-Ray Microscopy for Full-Field Nano Imaging of Biomaterials. Microsc Res Tech. 2011;74(7):671-81. doi: 10.1002/jemt.20907. PubMed PMID: WOS:000292570900011.
49. Maire E, Withers PJ. Quantitative X-ray tomography. International Materials Reviews. 2014;59(1):1-43. doi: 10.1179/1743280413y.0000000023. PubMed PMID: WOS:000330498000001.
50. Geng CX, Dunn PE. Hemostasis in Larvae of Manduca Sexta: Formation of a fibrous Coagulum by Hemolymph Proteins. Biochem Biophys Res Commun. 1988;155(2):1060-5. doi: 10.1016/s0006-291x(88)80604-1. PubMed PMID: WOS:A1988Q050400077.
51. Geng C. Studies of hemolymph coagulation in Manduca sexta. 1990.
52. Wigglesworth VB. Wound healing in an insect *(Rhodnius prolixus*, Hemiptera). Journal of Experimental Biology. 1937;14(3):364-81. PubMed PMID: WOS:000200577900010.
53. Green SM, Tobolsky AV. A new approach to the theory of relaxing polymeric media. Journal of Chemical Physics. 1946;14:80-92.
54. Plateau J. Statique Experimentale et The´orique des Liquides Soumis aux Seules Forces Mole´culaires. Paris,: Gauthier–Villars,; 1873.
55. Steinberg MS. Differential adhesion in morphogenesis: a modern view. Current Opinion in Genetics & Development. 2007;17(4):281-6. doi: 10.1016/j.gde.2007.05.002. PubMed PMID: WOS:000249366400004.
56. Foty RA, Steinberg MS. Differential adhesion in model systems. Wires Dev Biol. 2013;2(5):631-45. PubMed PMID: WOS:000323306600004.
57. Gonzalez-Rodriguez D, Guevorkian K, Douezan S, Brochard-Wyart F. Soft Matter Models of Developing Tissues and Tumors. Science. 2012;338(6109):910-7. doi: 10.1126/science.1226418. PubMed PMID: WOS:000311083600035.
58. Beaune G, Stirbat TV, Khalifat N, Cochet-Escartin O, Garcia S, Gurchenkov VV, et al. How cells flow in the spreading of cellular aggregates. Proceedings of the National Academy of Sciences of the United States of America. 2014;111(22):8055-60. doi: 10.1073/pnas.1323788111. PubMed PMID: WOS:000336687900051.
59. Janmey PA, Winer JP, Weisel JW. Fibrin gels and their clinical and bioengineering applications. Journal of the Royal Society Interface. 2009;6(30):1-10. doi: 10.1098/rsif.2008.0327. PubMed PMID: WOS:000262756800001.
60. Patteson AE, Asp ME, Janmey PA. Materials science and mechanosensitivity of living matter. Appl Phys Rev. 2022;9(1). doi: 10.1063/5.0071648. PubMed PMID: WOS:000783171000001.
61. Beris AN, Horner JS, Jariwala S, Armstrong MJ, Wagner NJ. Recent advances in blood rheology: a review. Soft Matter. 2021;17(47):10591-613. doi: 10.1039/d1sm01212f. PubMed PMID: WOS:000719451600001.

62. Scherfer C, Karlsson C, Loseva O, Bidla G, Goto A, Havemann J, et al. Isolation and characterization of hemolymph clotting factors in Drosophila melanogaster by a pullout method. Current Biology. 2004;14(7):625-9. doi: 10.1016/j.cub.2004.03.030. PubMed PMID: WOS:000220809900030.
63. Lesch C, Theopold U. Methods to study hemolymph clotting in insects. Insect Immunology. 2008:1-12.
64. Macosko CW. Rheology: Principles, Measurements, and Applications. New York: Wiley-VCH; 1994.
65. Haward SJ, Sharma V, Odell JA. Extensional opto-rheometry with biofluids and ultra-dilute polymer solutions. Soft Matter. 2011;7(21):9908-21. doi: 10.1039/c1sm05493g. PubMed PMID: WOS:000296026700017.
66. Entov VM, Hinch EJ. Effect of a spectrum of relaxation times on the capillary thinning of a filament of elastic liquid. J Non-Newton Fluid Mech. 1997;72(1):31-53. doi: 10.1016/s0377-0257(97)00022-0. PubMed PMID: WOS:A1997XP64400002.
67. Erickson HP. Size and shape of protein molecules at the nanometer level determined by sedimentation, gel filtration, and electron microscopy. Biological Procedures Online. 2009;11:32-51. doi: 10.1007/s12575-009-9008-x. PubMed PMID: 19495910.
68. He Y, Cao XL, Zhang SG, Rogers J, Hartson S, Jiang HB. Changes in the Plasma Proteome of Manduca sexta Larvae in Relation to the Transcriptome Variations after an Immune Challenge: Evidence for High Molecular Weight Immune Complex Formation. Molecular & Cellular Proteomics. 2016;15(4):1176-87. doi: 10.1074/mcp.M115.054296. PubMed PMID: WOS:000373992600001.
69. Arakawa T, Kato Y, Hattori M, Yamakawa M. Lipophorin: A carrier for lipids in insects participates in superoxide production in the haemolymph plasma. Insect Biochemistry and Molecular Biology. 1996;26(4):403-9. doi: 10.1016/0965-1748(95)00110-7. PubMed PMID: WOS:A1996UQ42100011.
70. Hoath SD, Vadillo DC, Harlen OG, McIlroy C, Morrison NF, Hsiao WK, et al. Inkjet printing of weakly elastic polymer solutions. J Non-Newton Fluid Mech. 2014;205:1-10. doi: 10.1016/j.jnnfm.2014.01.002. PubMed PMID: WOS:000333857000001.
71. Yan XJ, Carr WW, Dong HM. Drop-on-demand drop formation of polyethylene oxide solutions. Physics of Fluids. 2011;23(10). doi: 10.1063/1.3643269. PubMed PMID: WOS:000296528000029.
72. Zhang Z, Peng F, Kornev KG. The Thickness and Structure of Dip-Coated Polymer Films in the Liquid and Solid States. Micromachines. 2022;13(7):982. PubMed PMID: doi:10.3390/mi13070982.
73. Ribeiro C, Brehélin M. Insect haemocytes: What type of cell is that? Journal of Insect Physiology. 2006;52:417-29. doi: 10.1016/j.jinsphys.2006.01.005. PubMed PMID: 16527302.
74. Lavine MD, Strand MR. Insect hemocytes and their role in immunity. Insect Biochemistry and Molecular Biology. 2002;32:1295-309. doi: 10.1016/B978-012373976-6.50004-5. PubMed PMID: 12225920.
75. Lai-Fook J. The repair of wounds in the integument of insects. Journal of insect physiology. 1966;12:195-226.
76. Brodland GW. The differential interfacial tension hypothesis (DITH): a comprehensive theory for the self-rearrangement of embryonic cells and tissues. J Biomech Eng-Trans ASME. 2002;124(2):188-97. doi: 10.1115/1.1449491. PubMed PMID: WOS:000175343800006.
77. Mattix B, Olsen TR, Gu Y, Casco M, Herbst A, Simionescu DT, et al. Biological magnetic cellular spheroids as building blocks for tissue engineering. Acta Biomater. 2014;10(2):623-9. doi: 10.1016/j.actbio.2013.10.021. PubMed PMID: WOS:000330921700006.
78. Gregoire CH. Blood coagulation in Arthropods. HI. Reactions of insect hemolymph to coagulation inhibitors of vertebrate blood. Biol Bull. 1953;104((3)):372-93. doi: 10.2307/1538491. PubMed PMID: BCI:BCI19532700027216.

79. Rowley AF, Ratcliffe NA. The granular cells of Galleria mellonella during clotting and phagocytic reactions in vitro. Tissue and Cell. 1976;8:437-46. doi: 10.1016/0040-8166(76)90004-5.
80. Arnold JW. The hemocytes of insects. In: Rockstein M, editor. The physiology of insecta. 5. 2nd ed. New York: Academic Press; 1974. p. 201-54
81. Pech LL, Strand MR. Granular cells are required for encapsulation of foreign targets by insect haemocytes. J Cell Sci. 1996;109:2053-60. PubMed PMID: WOS:A1996VC21500009.
82. Pech LL, Strand MR. Plasmatocytes from the moth Pseudoplusia includens induce apoptosis of granular cells. Journal of Insect Physiology. 2000;46(12):1565-73. doi: 10.1016/s0022-1910(00)00083-4. PubMed PMID: WOS:000090079400007.
83. Bulgakova NA, Klapholz B, Brown NH. Cell adhesion in Drosophila: versatility of cadherin and integrin complexes during development. Current Opinion in Cell Biology. 2012;24(5):702-12. doi: 10.1016/j.ceb.2012.07.006. PubMed PMID: WOS:000310943300019.
84. Carthew RW. Adhesion proteins and the control of cell shape. Current Opinion in Genetics & Development. 2005;15(4):358-63. doi: 10.1016/j.gde.2005.06.002. PubMed PMID: WOS:000231205400002.
85. Godt D, Tepass U. Drosophila oocyte localization is mediated by differential cadherin-based adhesion. Nature. 1998;395(6700):387-91. doi: 10.1038/26493. PubMed PMID: WOS:000076083800055.
86. Hayashi T, Carthew RW. Surface mechanics mediate pattern formation in the developing retina. Nature. 2004;431(7009):647-52. doi: 10.1038/nature02952. PubMed PMID: WOS:000224299300030.
87. Machalowski T, Jesionowski T. Hemolymph of molluscan origin: from biochemistry to modern biomaterials science. Applied Physics a-Materials Science & Processing. 2021;127(1). doi: 10.1007/s00339-020-04166-1. PubMed PMID: WOS:000597637300001.
88. Stoepler TM, Castillo JC, Lill JT, Eleftherianos I. Hemocyte Density Increases with Developmental Stage in an Immune-Challenged Forest Caterpillar. Plos One. 2013;8(8). doi: 10.1371/journal.pone.0070978. PubMed PMID: WOS:000324401500055.
89. League GP, Hillyer JF. Functional integration of the circulatory, immune, and respiratory systems in mosquito larvae: pathogen killing in the hemocyte-rich tracheal tufts. Bmc Biology. 2016;14. doi: 10.1186/s12915-016-0305-y. PubMed PMID: WOS:000383839100001.
90. Sun Y, Ma J, Peng F, Kornev KG. Making droplets from highly viscous liquids by pushing a wire through a tube. Physics of Fluids. 2022;34(3). doi: 10.1063/5.0082003.
91. Sun YM, Bazilevsky AV, Kornev KG. Classification of axisymmetric shapes of droplets on fibers. Could non-wettable fibers support axisymmetric droplets? Physics of Fluids. 2023;35(7). doi: 10.1063/5.0151950. PubMed PMID: WOS:001025235200004.